Diagnostic Microbiology & Infectious Disease 109 (2024) 116298

Contents lists available at ScienceDirect

Diagnostic Microbiology & Infectious Disease

journal homepage: www.elsevier.com/locate/diagmicrobio

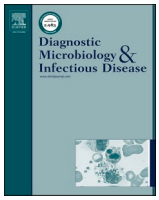

Antigen-functionalized turnip mosaic virus nanoparticles increase antibody sensing in saliva. A case study with SARS-CoV-2 RBD

Carlos Medrano-Arranz, Sara Rincón, Lucía Zurita, Fernando Ponz *, Daniel A. Truchado

Centro de Biotecnología y Genómica de Plantas, Universidad Politécnica de Madrid (UPM) – Instituto Nacional de Investigación Agraria y Alimentaria (INIA/CSIC), Campus de Montegancedo UPM, 28223 Pozuelo de Alarcón, Madrid, Spain

ARTICLE INFO

Keywords:
Turnip mosaic virus
SARS-CoV-2
VLP
Antibody sensing
Saliva;IgA

ABSTRACT

Nanoparticles derived from plant viruses play an important role in nanomedicine due to their biocompatibility, self-assembly and easily-modifiable surface. In this study, we developed a novel platform for increasing antibody sensing using viral nanoparticles derived from turnip mosaic virus (TuMV) functionalized with SARS-CoV-2 receptor binding domain (RBD) through three different methods: chemical conjugation, gene fusion and the SpyTag/SpyCatcher technology. Even though gene fusion turned out to be unsuccessful, the other two constructs were proven to significantly increase antibody sensing when tested with saliva of patients with different infection and vaccination status to SARS-CoV-2. Our findings show the high potential of TuMV nanoparticles in the fields of diagnostics and immunodetection, being especially attractive for the development of novel antibody sensing devices.

1. Introduction

Plant viral nanoparticles (VNP) have become very popular in biomedicine [1–5] due to their biosafety and their straightforward, cost-effective production. One example of this are VNPs derived from turnip mosaic virus (TuMV), a well-studied potyvirus with a great biotechnological potential [6,7]. The structure of TuMV VNPs consists of a flexuous, elongated capsid composed of approximately 2,000 copies of one capsid protein (CP; ≈ 33 kDa) helically assembled. There are two types of TuMV VNPs: virions, with capsid and genomic RNA; and empty virus-like particles (eVLP), formed only by self-assembled CPs and without the ability to infect. The structure and arrangement of the TuMV CP as well as the architecture of its capsid have been analyzed in detail through advanced computational methodologies and CryoEM [8–10]. All this knowledge has allowed the straightforward functionalization of TuMV VNPs via chemical conjugation [11–15], genetic engineering [16, 17] and the SpyTag/SpyCatcher technology [18]. In this study, we aimed at the functionalization of TuMV VNPs with the receptor-binding domain (RBD) of SARS-CoV-2 through the three different aforementioned strategies in order to develop a nanotool for increased IgA detection in saliva.

SARS-CoV-2 is a highly transmissible coronavirus that caused the largest pandemic in the 21st century [19]. Infection and vaccination against SARS-CoV-2 generate specific neutralizing antibodies against the RBD of the spike (S) protein [20,21] following the same pattern as with other viruses. Immunoglobulin M (IgM) is the first to be produced, whereas IgG and IgA become more present as levels of IgM decrease. While IgGs are predominant in plasma, IgAs are secreted mainly in the mucous membranes to prevent the entry of the virus into the body [22, 23]. In saliva, the production of IgA after vaccination alone is not as strong as after infection [24]. The immune status of a patient can be analyzed using either serum or saliva, given the strong correlation between RBD-specific immunoglobulins in both fluids [25]. Moreover, saliva, unlike serum, is easier to sample and gives also a view about mucosal immune response [26] although the concentration of Igs are lower than in serum, making necessary the improvement of antibody sensing [27].

Several functionalized VNPs for signal amplification have been developed during the last decades [28–32]. Nanotools derived from plant VNPs, have also been described for increased antigen sensing [33, 34] but, to our knowledge, only TuMV has been functionalized to increase antibody sensing. We demonstrated that TuMV VNPs are good candidates for that when functionalized with the appropriate epitope [35,17,36]. In this case, we propose the chemical conjugation of TuMV virions, and both genetic engineering and the SpyTag/SpyCatcher technology applied to eVLPs to compare three different alternatives to

* Corresponding author.
E-mail address: fponz@inia.csic.es (F. Ponz).

https://doi.org/10.1016/j.diagmicrobio.2024.116298
Received 23 January 2024; Received in revised form 3 April 2024; Accepted 3 April 2024
Available online 7 April 2024

obtain nanoparticles functionalized with the RBD of SARS-CoV-2. We hypothesized that RBD would increase its effective concentration when conjugated to TuMV nanoparticles, thus enhancing anti-RBD IgA sensing in saliva. To that end, we tested the viable constructs for IgA sensing using saliva of volunteers with different infection and vaccination status.

2. Material and methods

2.1. Chemical conjugation construct

In this experiment, we used purified TuMV virions and commercial RBD of SARS-CoV-2 (Agrenvec, Spain). This recombinant RBD protein (11.1 kDa) was produced by transient expression in non-transgenic plants. For this chemical conjugation, Staudinger reaction was used as described elsewhere [15] using NHS-phosphine and NHS-azide (Thermo Scientific, Germany) as linkers (Fig. S1).

To select the most effective chemical conjugation, two combinations were performed in parallel: TuMV-NHS-phosphine + RBD-NHS-azide and TuMV-NHS-azide + RBD-NHS-phosphine. First, the linkers were conjugated in a 5-fold molar excess with respect to TuMV CP and RBD. Then, TuMV-linker was bound to a 3-fold molar excess of RBD-linker. The excess of linker for RBD-linker was removed by centrifugal filters (Amicon ® Ultra – 0,5 mL Centrifugal Units 3 kDa, Merck Millipore, Germany) while the rest of excess were removed by ultracentrifugation (70,000 × g for 2 hours at 4°C). All samples were resuspended in 100 μL 10 mM HEPES buffer.

We performed an indirect enzyme-linked immunosorbent assay (ELISA) to check the correct conjugation and its efficiency. We coated high binding plates (Fisher Scientific, USA) with 5 μL of each construct (≈ 5 μg of TuMV-RBD) and 195 μL of 50 mM sodium carbonate buffer, pH 9.6. Serial dilutions of commercial free RBD in the same carbonate buffer were used as a reference to estimate the efficiency of the conjugation. After an overnight incubation at 4°C, we blocked with BSA 0.2 % in 50 mM sodium carbonate buffer, pH 9.6 for 1 h at 37°C. Then, samples were incubated with a 1:200 dilution of anti-POTY (Agdia, USA) or a 1:500 dilution of anti-RBD (R&D Systems, USA). The secondary antibody was a 1:500 dilution of anti-mouse conjugated to alkaline phosphatase (Agdia, USA) in both cases. All antibodies were diluted in PBS, 0.05 % Tween 20, 2 % PVP-40, 2 mg/mL BSA; and incubations took place for 1 h at 37°C. Alkaline phosphatase activity was observed using nitrophenylphosphate, and samples were measured at 405 nm (SPECTROstar Nano®; BMG Labtech, Germany).

2.2. Genetic fusion and SpyTag/SpyCatcher constructs

2.2.1. Cloning in expression vectors and infiltration in plants

Five different synthetic genes were designed (Fig. S2) and ordered from GenArt (Thermo Fisher Scientific, Germany). In all cases, the sequence of the RBD belonged to the original SARS-CoV-2 strain from Wuhan (WH-Human-1, GenBank accession number: NC_045512). All synthetic genes were cloned in the pEAQ-HT-DEST1 vector [37] and *Escherichia coli* top 10 cells (Thermo Fisher Scientific, Germany) to eventually transform cultures of *Agrobacterium tumefaciens* LBA4404 strains. Each construct was transiently expressed by agroinfiltration of *Nicotiana benthamiana* plants following a protocol described elsewhere [18].

2.2.2. Protein extraction and eVLP characterization

All agroinfiltrated leaves were harvested at 6 dpi. Crude extracts were obtained by mixing ≈ 75 mg of agroinfiltrated tissue with 250 μL of protein extraction buffer (50 mM Tris-HCl, pH 7.25; 150 mM NaCl; 2 mM EDTA; 0.1 % (v/v) Triton-X-100 and 1× SIGMAFAST™ protease inhibitor) using a tissue grinder. Aliquots of crude extracts were immediately frozen in liquid nitrogen and stored at -80°C until used.

To confirm the production of eVLPs via genetic fusion, we performed the same ELISA protocol as with the chemical conjugated construct. In the case of the SpyTag/SpyCatcher constructs, TEM was applied to check the binding of RBD to the eVLPs. To that end, 400 mesh copper-carbon-coated electron microscopy grids were floated with 10 μL of crude extract at RT for 10 min. Then, the grids were washed with five drops of distilled H_2O for 5 min each and incubated, for 10 min, with a 1:1000 dilution of anti-POTY (Agdia, USA) or anti-RBD (R&D Systems, USA) in 50 mM borate buffer, pH 8.1. After that, the grids were washed in distilled H_2O and incubated with 10 μL of a 1:50 dilution of 5 nm gold-labelled anti-mouse antibody (Sigma, USA) in 50 mM borate buffer, pH 8.1 for 10 min. Finally, all the grids were rinsed five times with distilled H_2O and stained with 2 % (w/v) uranyl acetate for 3 min. Grids were eventually examined on a transmission electron microscope (JEM JEOL 1400, Tokyo, Japan) in an external service (TEM, ICTS-CNME, Madrid, Spain).

2.3. Antibody detection in saliva by ELISA

Saliva samples of four volunteers (Table 1) were centrifuged at 2,700 × g for 10 min and diluted 1:16 in PBS. We coated high binding plates (Fisher Scientific, USA) with 5 μL of each construct and 195 μL of 50 mM sodium carbonate buffer, pH 9.6. The positive control consisted of 15 μg/well of free commercial RBD, a sufficient amount to saturate the well (Fig. S3). A negative control of crude extract from a non-agroinfiltrated *Nicotiana benthamiana* leaf was added in the ELISA of SpyTag/SpyCatcher construct. Coating was carried out for 2 h at 37°C. After 3 washes with PBS-Tween, we blocked the wells using 50 μL of BSA 2 % in 50 mM sodium carbonate buffer, pH 9.6 for 1 h at 37°C. After 3 washes with PBS-Tween, 50 μL of the 1:16 dilution of saliva was added to each well, incubating overnight at 4°C. Then, we washed the plate 6 times with PBS-Tween and samples were incubated with a 1:20,000 dilution of anti-human IgA conjugated to HRP (Invitrogen, UK) for 1 h at 37°C. Finally, the plate was washed 3 times with PBS-Tween and HRP activity was detected using 50 μL of TMB (Ultra-TMB, Thermo Scientific, Germany). Reaction was stopped after 5 min using 50 μL of HCl 2 N. Absorbance at 450 nm was measured in a microplate reader (SPECTROstar Nano®; BMG Labtech, Germany).

A second ELISA was performed to discard false positives with the SpyTag/SpyCatcher construct. We also re-checked the saliva of those subjects who were unexpectedly positive in the first ELISA, four months afterwards. We added three extra negative controls: crude extract from a leaf agroinfiltrated with non-functionalized eVLP and two saliva samples taken in February 2019, prior to the COVID-19 pandemic onset. Samples and data from patients included in this study were provided by the Biobank Biobanco Hospital Universitario de La Princesa (Madrid) (ISCIII B.0000763) and they were processed following standard operating procedures with the appropriate approval of the Ethics and Scientific Committees.

3. Results

3.1. Chemical conjugation construct

Indirect ELISA incubated with anti-RBD revealed that only the TuMV-phosphine + RBD-azide construct was successfully functionalized (Fig. 1A), in which a RBD concentration of 5.33 μM was estimated.

Table 1
Information about the four volunteers whose saliva was analyzed in this study.

Subject	Testing dates	Last dose of SARS-CoV-2 vaccine	Last SARS-CoV-2 infection
1	May 2023	February 2022	April 2023
2	May 2023	March 2023	October 2022
3	May 2023	October 2022	November 2022
4	May and December 2023	August 2021	Not known

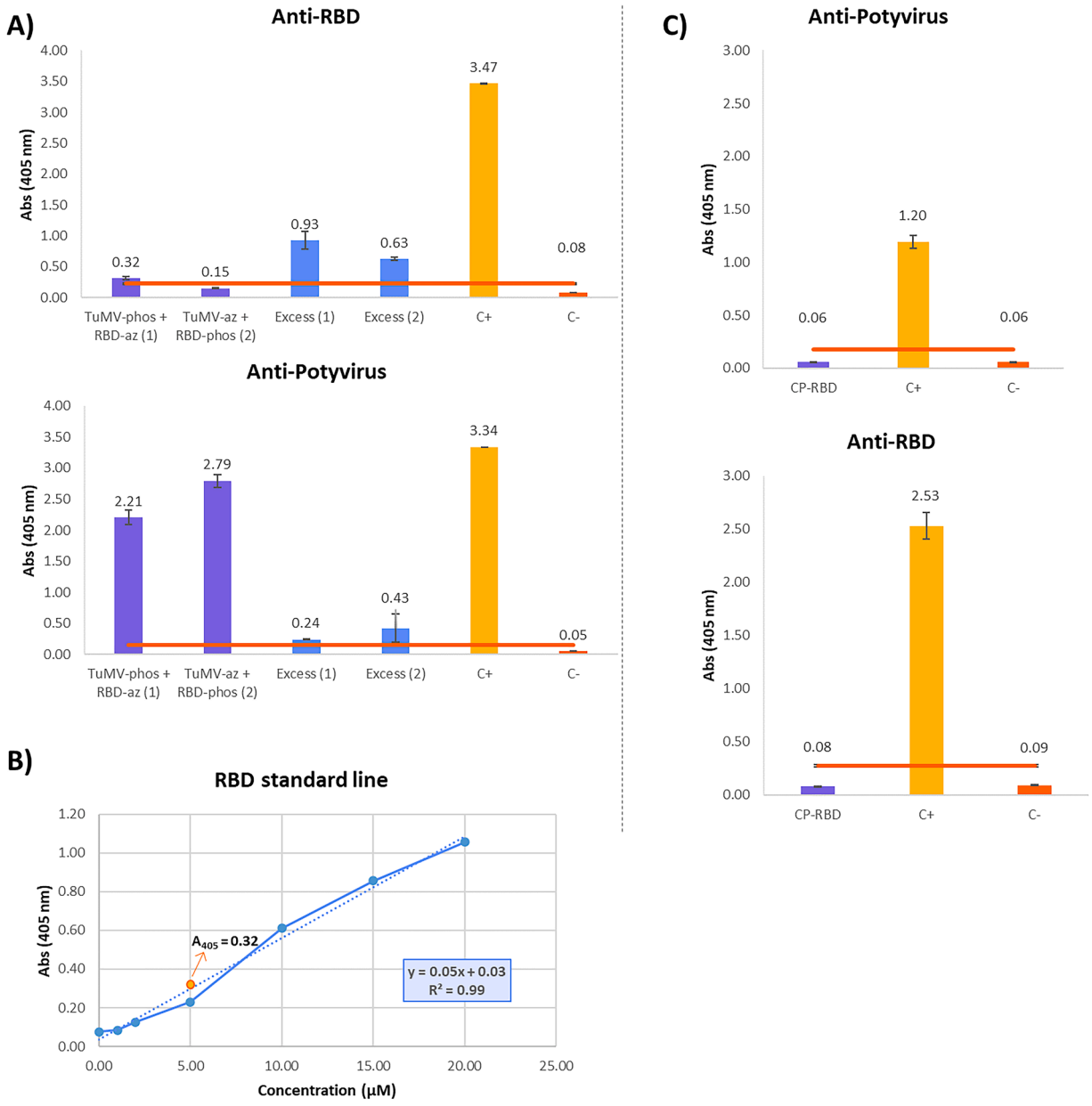

Fig. 1. (A) Indirect ELISA results to check for the correct functionalization of TuMV virions with RBD by chemical conjugation. The lower graph shows the results with anti-potyvirus as primary antibody; the upper graph shows the results using anti-RBD. The orange horizontal line indicates the threshold at which a positive absorbance is considered, which was set at three times the value of the negative control. All samples were analyzed in triplicate. The error bars show the standard deviation. (B) RBD standard line obtained through an indirect ELISA and serial dilutions of the free protein. The value of the sample TuMV-phosphine + RBD-azide is highlighted. Az: NHS-azide linker; phos: NHS-phosphine linker; TuMV: turnip mosaic virus; RBD: SARS-CoV-2 receptor-binding domain; Excess (1): supernatant of the ultracentrifugation of the TuMV-phosphine + RBD-azide combination; Excess (2): supernatant of the ultracentrifugation of the TuMV-azide + RBD-phosphine combination. C) Indirect ELISA results to check for correct functionalization by gene fusion. The upper graph shows the results with anti-potyvirus; the lower graph shows the results with anti-RBD. The orange horizontal line indicates the threshold, which was set at three times the value of the negative control. The error bars show the 95% confidence interval for the absorbance values. CP: turnip mosaic virus capsid protein; RBD: SARS-CoV-2 receptor-binding domain.

Considering that a TuMV virion has approximately 2,000 CPs, it means that ≈ 360 RBD molecules per virion were conjugated (Fig. 1B). As the molecular weight of RBD was 11.1 kDa, it was thus estimated that 5 µL of conjugated TuMV-RBD contained approximately 0.3 µg of RBD.

3.2. Genetic fusion and SpyTag/SpyCatcher constructs

The indirect ELISA showed a negative result for the production of the genetic fusion construct (Fig. 1C).

For both SpyTag/SpyCatcher constructs, we observed assembled eVLPs in TEM micrographs. However, only the SpyCatcher-CP + SpyTag-RBD construct eVLPs were decorated with colloidal gold, showing a successful functionalization with RBD (Fig. 2). Therefore, we selected only this construct for the IgA detection by ELISA.

3.3. Antibody detection in saliva by ELISA

Both constructs (chemical conjugation and SpyTag/SpyCatcher) outperformed the positive control containing the same amount of free RBD as the estimated for the chemical conjugation. However, the SpyTag/Spy Catcher construct resulted more sensitive than the chemical conjugation. These differences were higher in subject 1 (most recently

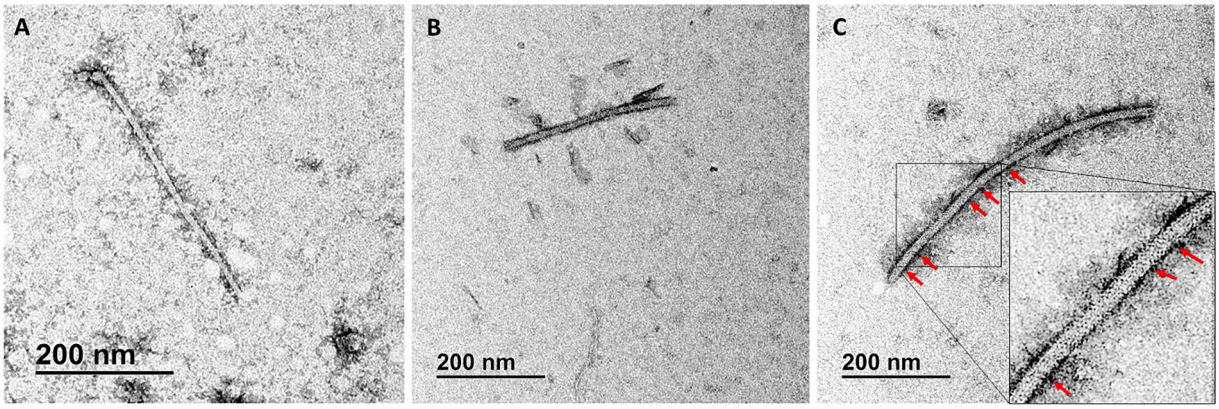

Fig. 2. TEM micrographs of functionalized VLP-RBD obtained through the SpyTag/SpyCatcher technology. (A) Functionalized VLP without decoration (Control); (B) SpyCatcher-RBD + SpyTag-CP; (C) SpyCatcher-CP + SpyTag-RBD. Red arrows highlight some of the distinguishable colloidal gold molecules.

infected by SARS-CoV-2), followed by subject 4 (no known infection). Subjects 2 and 3, who were infected by SARS-CoV-2 more than 6 months prior to the analysis, showed the lowest absorbance values (Fig. 3).

Focusing on the ELISA of the SpyTag/SpyCatcher construct, absorbance values were significantly higher than the free RBD positive control in saturation. All negative controls showed lower absorbances than the construct (Figs. 4 and S4).

4. Discussion

Currently, immunity status against SARS-CoV-2 is assessed primarily through antibody titers in serum. Nevertheless, we developed functionalized TuMV nanoparticles that could be alternatively used to develop a platform for antibody sensing in saliva, a less invasive method for the patient.

The use of VNPs for antibody sensing was not as popular as other applications in nanomedicine such as antigen detection [38,29–32,39]. Although plant viruses have also been successfully functionalized to

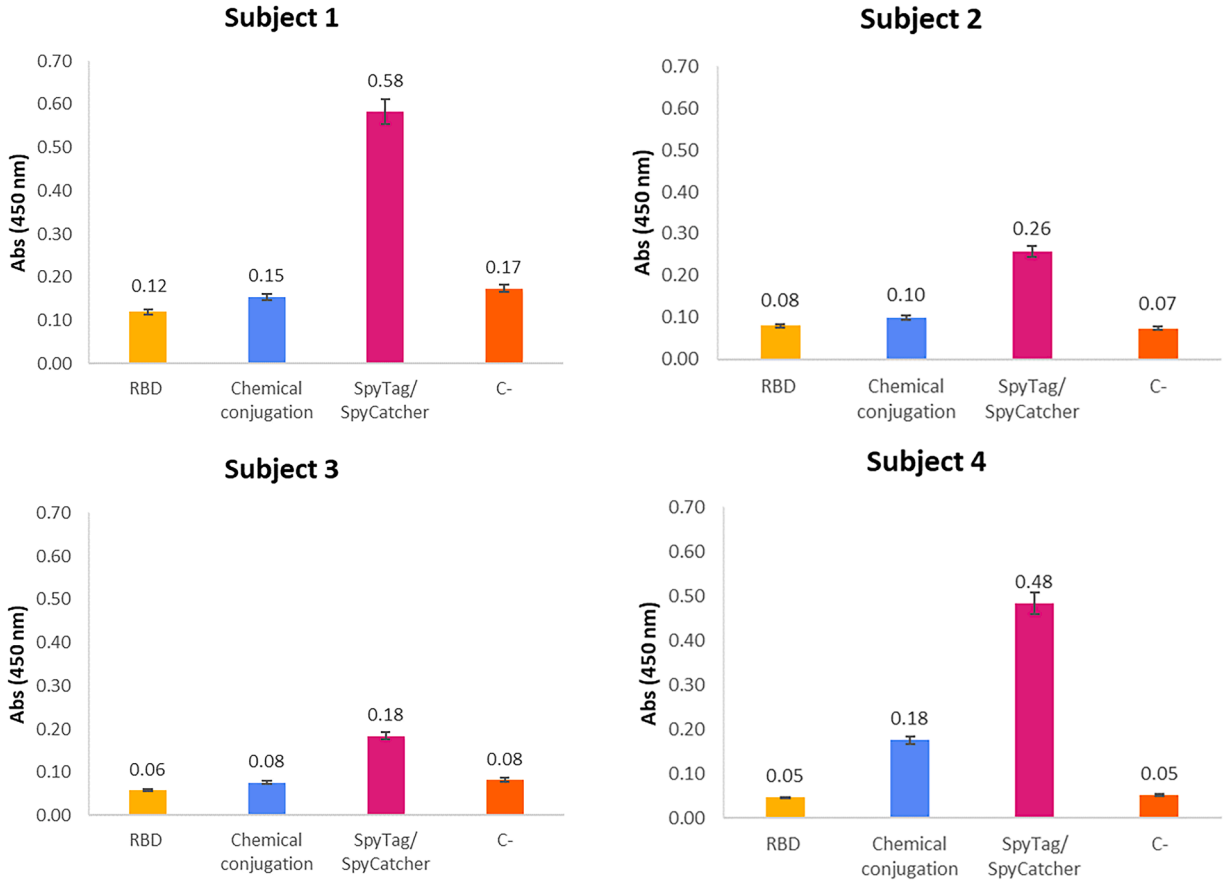

Fig. 3. Indirect ELISA results for the detection of anti-RBD IgA in saliva by the functionalized TuMV nanoparticles analyzed in this study. Yellow bars represent the positive control containing the same amount of free RBD as the estimated for the chemical conjugation (0.3 μg). Blue bars show the detection when coating with the chemically conjugated TuMV-RBD virions. Pink bars show the detection when coating with the eVLPs functionalized with RBD via SpyTag/SpyCatcher technology. Orange bars are the negative control with no coating. The error bars show the 95% confidence interval for the absorbance values.

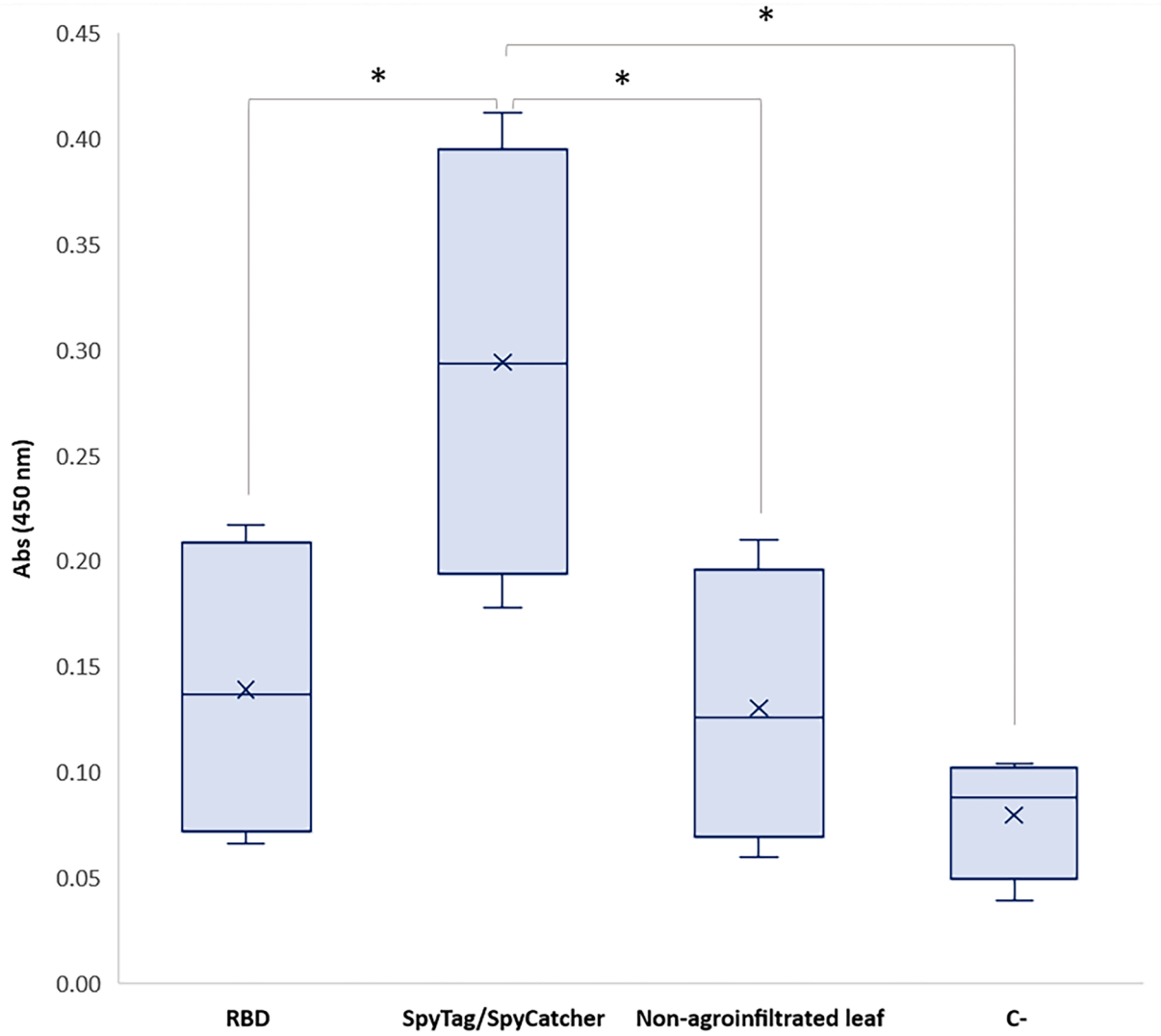

Fig. 4. Box-and-whisker plot with the results of the indirect ELISA carried out to check the different IgA detection capacity in saliva between the SpyTag/SpyCatcher construct and free commercial RBD. The saliva of the four volunteers analyzed in this study (subjects 1, 2, 3 and 4) was used as the primary antibody. A negative control consisting in the crude extract of a non-agroinfiltrated leaf was used to rule out a false positive due to possible peroxidase activity present in *Nicotiana benthamiana* leaves. C-: negative control with no coating. The results were compared by a t-test (* $p < 0.05$; ** $p < 0.01$; *** $p < 0.001$).

increase the detection of antigens [33,34], we proved that TuMV nanoparticles were especially convenient to increase antibody sensing given their capsid architecture [35,17,36].

We first tested whether the way in which the TuMV nanoparticles were functionalized might influence the sensitivity in IgA detection. Genetic fusion resulted unsuccessful as we could not confirm the production of eVLPs in the plant. The same outcome was reported before for TuMV eVLPs when this functionalization technique was tested with the vasoactive intestinal peptide (VIP) [15]. Advanced computational analyses revealed that the composition of VIP and its interactions with the CP in the fusion protein hampered the mobility of the N-terminal arm, a key element for VNPs assembly [9]. Such analyses have not been performed for RBD, but it is highly likely that this peptide interferes somehow with the structural intrinsic disorder of the CP N-terminal arm, thus abolishing the formation of eVLPs. However, the two constructs that we successfully obtained resulted more sensitive to detect anti-RBD IgAs in saliva than the free antigen. It was remarkable that only 5 μL of crude extract with the SpyTag/SpyCatcher construct were significantly more sensitive than free RBD in saturation. These results are in line with those shown in previous studies using TuMV functionalized with small peptides. In those cases, coating with the functionalized TuMV nanoparticles also enhanced antibody detection compared to coating with the same amount of free peptide [35,17]. Therefore, this study supports the application of functionalized TuMV nanoparticles to increase antibody sensing in saliva as well. This increased antibody sensing could be explained by the multimeric display of the antigen in a potyvirus scaffold, which creates a dense and repetitive arrangement of the peptide recognized by the antibodies that cannot be matched when the peptide is free in solution.

Regarding the SpyTag/SpyCatcher eVLPs, we demonstrated the correct assembly in both cases, although we could not observe a successful functionalization with SpyCather-RBD. Generally, when all possible combinations between SpyTag and SpyCatcher are tested with the CP and the protein of interest, there is always one functionalization that occurs in a minor way or not at all [40,18]. In our study, perhaps SpyCatcher-RBD was produced in a low quantity and was not easily detectable or the construct might have been degraded by plant proteases. Either way, the alternative construct with SpyTag-RBD turned out to be the most sensitive one. This result may be explained because chemical conjugation is not as efficient in some cases [15]. According to our estimation, only 18 % of the CPs of the virions would have been functionalized with a RBD molecule, being this the possible reason why

this construct was not as sensitive as the alternative. These outcomes suggest that the SpyTag/SpyCatcher technology was the best option to functionalize the TuMV nanoparticles with RBD for antibody sensing. This technology, based on the isopeptide bond that occurs spontaneously between the peptides SpyTag and SpyCatcher [41], turned out to be the best approach when chemical conjugation was not very efficient and genetic fusion was not viable [18]. However, its major drawback is the lack of a purification protocol for flexuous eVLPs. This leads to the use of crude extracts for the analyses, giving high background absorbance levels due to undesired interactions between proteins. Nevertheless, the sensitivity of only 5 μL of crude extract was significantly higher than the positive control saturated with RBD.

Our results also revealed a good reliability of the detection, as the highest readings corresponded to the subject with a recent infection and the lowest readings to those who passed the COVID more than 3 months prior to the analysis, which is in line with previous analysis [25,27,42]. The case of subject 4, with no known SARS-CoV-2 infection, may be explained by an asymptomatic infection that went undetected. This is supported by the fact that, four months later, the saliva from this subject was still positive to IgA against RBD while all negative controls ruled out the possibility of false positives. Also, it is highly unlikely to observe such high IgA levels in saliva more than one year after the second dose of mRNA vaccine [24]. Thus, we show that the functionalized nanoparticles we developed were also able to assess the immune status of patients who may have had an asymptomatic infection and do not know whether they still have enough antibodies against the virus.

A limitation of our approach in its current stage of development is the use of plant extracts instead of purified nanoparticles, due to the absence of good available purification protocols for plant flexuous elongated VLPs. This may lead to non-specific interactions in the ELISA with the consequence of the need of a large number of negative controls to monitor them. Another characteristic of this study was the low number of patients tested. Considering its proof-of-concept posing, the study has shown the high potential of the VLP approach. For the future then, the development of devices based on TuMV nanoparticles for the detection of antibodies in saliva should focus on establishing VLP purification protocols, and the number of patients tested should be sufficient to cover all possible immunological situations.

5. Conclusion

Functionalized TuMV VNPs are a promising nanotool for IgA detection in saliva. They showed increased antibody sensing and were able to detect IgAs even in cases of low antibody titers, where the free antigen failed. This together with their low-cost production and their straightforward functionalization with antigens make them attractive for the development of devices for rapid antibody detection in saliva or other biofluids with low antibody titers.

CRediT authorship contribution statement

Carlos Medrano-Arranz: Investigation. **Sara Rincón:** Investigation. **Lucía Zurita:** Investigation. **Fernando Ponz:** Writing – review & editing, Supervision, Methodology, Funding acquisition, Conceptualization. **Daniel A. Truchado:** Writing – original draft, Methodology, Investigation, Conceptualization.

Declaration of competing interest

The authors declare that they have no known competing financial interests or personal relationships that could have appeared to influence the work reported in this paper

Acknowledgements

This work was mostly funded by grant COV20/00114 from Comunidad de Madrid to FP. We want to particularly acknowledge the donors and the Biobank Biobanco Hospital Universitario de La Princesa (Madrid) (ISCIII B.0000763) for their collaboration. We also thank Agrenvec S.L (Tres Cantos, Madrid, Spain) for the generous gift of its plant-made RBD. DAT was supported by a Margarita Salas postdoctoral grant funded by the Spanish Ministry of Universities and UCM (CT31/21). SR was funded by a contract under grant P2018/BAA-4574 from the Comunidad de Madrid. This work was part of the Final Grade Thesis of CM for graduation in biotechnology by the UPM. The CBGP was granted 'Severo Ochoa' Distinctions of Excellence by the Spanish Ministry of Science and Innovation (SEV- 2016-0672 and CEX2020-000999-S).

Supplementary materials

Supplementary material associated with this article can be found, in the online version, at doi:10.1016/j.diagmicrobio.2024.116298.

References

[1] Chung YH, Cai H, Steinmetz NF. Viral nanoparticles for drug delivery, imaging, immunotherapy, and theranostic applications. Adv Drug Deliv Rev 2020;156:214–35. https://doi.org/10.1016/j.addr.2020.06.024.
[2] Rybicki EP. Plant molecular farming of virus-like nanoparticles as vaccines and reagents. Wiley Interdiscip Rev Nanomedicine Nanobiotechnology 2020;12. https://doi.org/10.1002/wnan.1587.
[3] Shukla S, Dickmeis C, Fischer R, Commandeur U, Steinmetz NF. In planta production of fluorescent filamentous plant virus-based nanoparticles. Method Mol Biol 2018;1776:61–84. https://doi.org/10.1007/978-1-4939-7808-3_5.
[4] Shukla S, Dickmeis C, Nagarajan AS, Fischer R, Commandeur U, Steinmetz NF. Molecular farming of fluorescent virus-based nanoparticles for optical imaging in plants, human cells and mouse models. Biomater Sci 2014;2:784–97. https://doi.org/10.1039/c3bm60277j.
[5] Wu Z, Jiajing Z, Nkanga CI, Jin Z, He T, Borum RM, et al. One-step supramolecular multifunctional coating on plant virus nanoparticles for bioimaging and therapeutic applications. ACS Appl Mater Interface 2022;14:13692–702. https://doi.org/10.1021/acsami.1c22690.
[6] Nellist CF, Ohshima K, Ponz F, Walsh JA. Turnip mosaic virus, a virus for all seasons. Ann Appl Biol 2022;180:312–27. https://doi.org/10.1111/aab.12755.
[7] Truchado DA, Rincón S, Zurita L, Ponz F. Turnip mosaic virus nanoparticles: a versatile tool in biotechnology. editors. In: Kole C, Chaurasia A, Hefferon KLPJ, editors. Tools tech. Plant mol. Farming. Concepts strateg. Plant sci. Singapore: Springer; 2023. p. 235–49. https://doi.org/10.1007/978-981-99-4859-8_8.
[8] Cuesta R, Yuste-Calvo C, Gil-Cartón D, Sánchez F, Ponz F, Valle M. Structure of Turnip mosaic virus and its viral-like particles. Sci Rep 2019;9. https://doi.org/10.1038/s41598-019-51823-4.
[9] Mínguez-Toral M, Pacios LF, Sánchez F, Ponz F. Structural intrinsic disorder in a functionalized potyviral coat protein as a main viability determinant of its assembled nanoparticles. Int J Biol Macromol 2023;236:123958. https://doi.org/10.1016/j.ijbiomac.2023.123958.
[10] Pacios LF, Sánchez F, Ponz F. Intrinsic disorder in the dynamic evolution of structure, stability, and flexibility of potyviral VLP assemblies: a computational study. Int J Biol Macromol 2024;254. https://doi.org/10.1016/j.ijbiomac.2023.127798.
[11] Cuenca S, Mansilla C, Aguado M, Yuste-Calvo C, Sánchez F, Sánchez-Montero JM, et al. Nanonets derived from turnip mosaic virus as scaffolds for increased enzymatic activity of immobilized *Candida antarctica* lipase B. Front Plant Sci 2016;7:464. https://doi.org/10.3389/fpls.2016.00464.
[12] González-Gamboa I, Velázquez-Lam E, Lobo-Zegers MJ, Frías-Sánchez AI, Tavares-Negrete JA, Monroy-Borrego A, et al. Gelatin-methacryloyl hydrogels containing turnip mosaic virus for fabrication of nanostructured materials for tissue engineering. Front Bioeng Biotechnol 2022;10:907601. https://doi.org/10.3389/fbioe.2022.907601.
[13] Velázquez-Lam E, Imperial J, Ponz F. Polyphenol-functionalized plant viral-derived nanoparticles exhibit strong antimicrobial and antibiofilm formation activities. ACS Appl Bio Mater 2020;3:2040–7. https://doi.org/10.1021/acsabm.9b01161.
[14] Velázquez-Lam E, Tome-Amat J, Segrelles C, Yuste-Calvo C, Asensio S, Peral J, et al. Antitumor applications of polyphenol-conjugated turnip mosaic virus-derived nanoparticles. Nanomedicine 2022:999–1012. https://doi.org/10.2217/nnm-2022-0067.
[15] Yuste-Calvo C, González-Gamboa I, Pacios LF, Sánchez F, Ponz F. Structure-based multifunctionalization of flexuous elongated viral nanoparticles. ACS Omega 2019;4:5019–28. https://doi.org/10.1021/acsomega.8b02760.
[16] Pazos-Castro D, Margain C, Gonzalez-Klein Z, Yuste-Calvo C, Garrido-Arandia M, Zurita L, et al. Suitability of potyviral recombinant virus-like particles bearing a complete food allergen for immunotherapy vaccines. Front Immunol 2022;13:986823. https://doi.org/10.3389/fimmu.2022.986823.
[17] Sánchez F, Sáez M, Lunello P, Ponz F. Plant viral elongated nanoparticles modified for log-increases of foreign peptide immunogenicity and specific antibody detection. J Biotechnol 2013;168:409–15. https://doi.org/10.1016/j.jbiotec.2013.09.002.

[18] Truchado DA, Rincón S, Zurita L, Sánchez F, Ponz F. Isopeptide bonding *in planta* allows functionalization of elongated flexuous proteinaceous viral nanoparticles, including non-viable constructs by other means. Viruses 2023;15:375. https://doi.org/10.3390/v15020375.
[19] Lamers MM, Haagmans BL. SARS-CoV-2 pathogenesis. Nat Rev Micro 2022;20:270–84. https://doi.org/10.1038/s41579-022-00713-0.
[20] Krammer F. SARS-CoV-2 vaccines in development. Nature 2020;586:516–27. https://doi.org/10.1038/s41586-020-2798-3.
[21] Yuan M, Liu H, Wu NC, Wilson IA. Recognition of the SARS-CoV-2 receptor binding domain by neutralizing antibodies. Biochem Biophys Res Commun 2021;538:192–203. https://doi.org/10.1016/j.bbrc.2020.10.012.
[22] Chao YX, Rötzschke O, Tan EK. The role of IgA in COVID-19. Brain Behav Immun 2020;87:182–3. https://doi.org/10.1016/j.bbi.2020.05.057.
[23] Lamm ME, Nedrud JG, Kaetzel CS, Mazanec MB. IgA and mucosal defense. APMIS 1995;103:241–6. https://doi.org/10.1111/j.1699-0463.1995.tb01101.x.
[24] Sheikh-Mohamed S, Isho B, Chao GYC, Zuo M, Cohen C, Lustig Y, et al. Systemic and mucosal IgA responses are variably induced in response to SARS-CoV-2 mRNA vaccination and are associated with protection against subsequent infection. Mucosal Immunol 2022;15:799–808. https://doi.org/10.1038/s41385-022-00511-0.
[25] Isho B, Abe KT, Zuo M, Jamal AJ, Rathod B, Wang JH, et al. Persistence of serum and saliva antibody responses to SARS-CoV-2 spike antigens in COVID-19 patients. Sci Immunol 2020;5. https://doi.org/10.1126/sciimmunol.abe5511.
[26] Sheikh-Mohamed S, Sanders EC, Gommerman JL, Tal MC. Guardians of the oral and nasopharyngeal galaxy: IgA and protection against SARS-CoV-2 infection*. Immunol Rev 2022;309:75–85. https://doi.org/10.1111/imr.13118.
[27] Guerra ENS, Castro VTd, Amorim dos Santos J, Acevedo AC, Chardin H. Saliva is suitable for SARS-CoV-2 antibodies detection after vaccination: A rapid systematic review. Front Immunol 2022;13. https://doi.org/10.3389/fimmu.2022.1006040.
[28] Charlermroj R, Makornwattana M, Phuengwas S, Karoonuthaisiri N. A rapid colorimetric lateral flow test strip for detection of live *Salmonella* Enteritidis using whole phage as a specific binder. Front Microbiol 2022;13. https://doi.org/10.3389/fmicb.2022.1008817.
[29] Domaille DW, Lee JH, Cha JN. High density dna loading on the m13 bacteriophage provides access to colorimetric and fluorescent protein microarray biosensors. Chem Commun 2013;49:1759–61. https://doi.org/10.1039/c3cc38871a.
[30] Lee JH, Cha JN. Amplified protein detection through visible plasmon shifts in gold nanocrystal solutions from bacteriophage platforms. Anal Chem 2011;83:3516–9. https://doi.org/10.1021/ac200222d.
[31] Lee JH, Xu PF, Domaille DW, Choi C, Jin S, Cha JN. M13 bacteriophage as materials for amplified surface enhanced raman scattering protein sensing. Adv Funct Mater 2014;24:2079–84. https://doi.org/10.1002/adfm.201303331.
[32] Liu J, Pang S, Wang M, Yu H, Ma P, Dong T, et al. An ultrasensitive ELISA to assay femtomolar level SARS-CoV-2 antigen based on specific peptide and tyramine signal amplification. Sensors Actuators B Chem 2023;387. https://doi.org/10.1016/j.snb.2023.133746.
[33] Guo J, Zhao X, Hu J, Lin Y, Wang Q. Tobacco mosaic virus with peroxidase-like activity for cancer cell detection through colorimetric assay. Mol Pharm 2018;15:2946–53. https://doi.org/10.1021/acs.molpharmaceut.7b00921.
[34] Martí M, Merwaiss F, Butković A, Daròs JA. Production of potyvirus-derived nanoparticles decorated with a nanobody in biofactory plants. Front Bioeng Biotechnol 2022;10. https://doi.org/10.3389/fbioe.2022.877363.
[35] González-Gamboa I, Manrique P, Manrique P, Ponz F. Plant-made potyvirus-like particles used for log-increasing antibody sensing capacity. J Biotechnol 2017;254:17–24. https://doi.org/10.1016/j.jbiotec.2017.06.014.
[36] Yuste-Calvo C, López-Santalla M, Zurita L, Cruz-Fernández CF, Sánchez F, Garín MI, et al. Elongated flexuous plant virus-derived nanoparticles functionalized for autoantibody detection. Nanomaterials 2019;9. https://doi.org/10.3390/nano9101438.
[37] Sainsbury F, Thuenemann EC, Lomonossoff GP. PEAQ: Versatile expression vectors for easy and quick transient expression of heterologous proteins in plants. Plant Biotechnol J 2009;7:682–93. https://doi.org/10.1111/j.1467-7652.2009.00434.x.
[38] Adhikari M, Dhamane S, Hagström AEV, Garvey G, Chen WH, Kourentzi K, et al. Functionalized viral nanoparticles as ultrasensitive reporters in lateral-flow assays. Analyst 2013;138:5584–7. https://doi.org/10.1039/c3an00891f.
[39] Mao C, Liu A, Cao B. Virus-based chemical and biological sensing. Angew Chemie - Int Ed 2009;48:6790–810. https://doi.org/10.1002/anie.200900231.
[40] Peyret H, Ponndorf D, Meshcheriakova Y, Richardson J, Lomonossoff GP. Covalent protein display on Hepatitis B core-like particles in plants through the in vivo use of the SpyTag/SpyCatcher system. Sci Rep 2020;10. https://doi.org/10.1038/s41598-020-74105-w.
[41] Reddington SC, Howarth M. Secrets of a covalent interaction for biomaterials and biotechnology: SpyTag and SpyCatcher. Curr Opin Chem Biol 2015;29:94–9. https://doi.org/10.1016/j.cbpa.2015.10.002.
[42] Marot S, Malet I, Leducq V, Zafilaza K, Sterlin D, Planas D, et al. Rapid decline of neutralizing antibodies against SARS-CoV-2 among infected healthcare workers. Nat Commun 2021;12. https://doi.org/10.1038/s41467-021-21111-9.